

SUPPLEMENTARY MATERIAL TO:

**On Mean Flow Universality of Turbulent Wall Flows.
II. Asymptotic Flow Analysis**

Stefan Heinz

University of Wyoming, Mathematics Department, Laramie, WY 82071, USA.

Details to the discussions in Sect. 3 are provided here: mean bulk flow properties (bulk velocity, skin-friction coefficient, and bulk Reynolds number) are considered in Suppl. S.1, and related turbulence properties (turbulence production and turbulent viscosity) are considered in Suppl. S.2. The particular goal is the derivation of asymptotic profiles of these variables and their comparison with corresponding models directly implied by the PVM.

S.1. Bulk Velocity, Skin-Friction Coefficient, and Bulk Reynolds Number

For all the three flows considered, the bulk velocity is defined by $U_b^+ = \int_0^1 U^+ dy$. Using integration by parts, this relation can be identically written as

$$U_b^+ = U^+(1) - \kappa^{-1} \int_0^1 \kappa y^+ S^+ dy = U^+(1) - \kappa^{-1}(I_{12} + I_3). \quad (\text{S.1})$$

Here, $U^+(1)$ refers to U^+ at $y = 1$, which is equivalent to U_∞^+ for channel and pipe flow, and $0.99U_\infty^+$ for the TBL. The last expression introduces $\int_0^1 \kappa y^+ S^+ dy = I_{12} + I_3$, where

$$I_{12} = \int_0^1 \kappa y^+ (S^+ - S_3^+) dy, \quad I_3 = \int_0^1 \kappa y^+ S_3^+ dy. \quad (\text{S.2})$$

The integral I_3 is a constant. Using numerical integration we find $I_3 = (-0.0258, 0.1248, 0.5217)$ for channel flow, pipe flow, and the TBL, respectively. The other integral I_{12} is a function of Re_τ .

For channel and pipe flow, I_{12} is affected by the outer boundary terms S_1^{CP} and S_2^{CP} . The effect of S_1^{CP} and S_2^{CP} on I_{12} given by Eq. (S.2) can be assessed in the following way. By using $|S_1^{CP}| \leq y S_1^+(1)$, see reference [25] (Supplementary Material, second paragraph), we find $\int_0^1 \kappa y^+ S_1^{CP} dy = -\gamma_1 \kappa Re_\tau S_1^+(1)/3$, where γ_1 is a proportionality coefficient. The numerical calculation of γ_1 proves that $\gamma_1 = 1$ represents a highly accurate approximation for $Re_\tau \geq 200$. Correspondingly, by using $|S_2^{CP}| \leq (1 - [\kappa Re_\tau S_2^+(1)]^{-1}) S_2^+(1)$, see reference [25] (Supplementary Material, last paragraph), we find $\int_0^1 \kappa y^+ S_2^{CP} dy = -\gamma_2 \kappa Re_\tau S_2^+(1)(1 - [\kappa Re_\tau S_2^+(1)]^{-1})/2$, where γ_2 is a proportionality coefficient. The numerical calculation of γ_2 shows that γ_2 is a function that varies between 0.94 and 1 for $Re_\tau \geq 500$. A very accurate approximation for γ_2 for the range $Re_\tau \geq 200$ is given by $\gamma_2 = (1 + \exp(-0.135[\ln Re_\tau]^2 + 0.211 \ln Re_\tau + 1.229))^{-1}$. Based on these expressions it is possible to prove that the effect of S_1^{CP} and S_2^{CP} on the calculation of U_b^+ is less than 0.09% for $Re_\tau \geq 500$.

Thus, the effect of S_1^{CP} and S_2^{CP} on I_{12} will be neglected in order to not unnecessarily complicate the calculation. In this case, I_{12} can be analytically obtained by following the developments made in reference [25] (Supplementary Material). We obtain

$$I_{12} = \frac{\kappa a^2}{2Re_\tau} \left[c B_{G_*} \left(c + \frac{2c}{b}, 1 - \frac{2c}{b} \right) + G_*^{\frac{2c}{b}} (1 - G_*)^{-\frac{2c}{b}} - G_*^{c + \frac{2c}{b}} (1 - G_*)^{-\frac{2c}{b}} \right] + J(p_*). \quad (\text{S.3})$$

The first and second contributions arise from the integration of $\kappa y^+ S_1^+$ and $\kappa y^+ S_2^+$, respectively. Here, G_* and p_* are obtained by setting $y^+ = Re_\tau$ in $G = (y^+/a)^{b/c}/[1 + (y^+/a)^{b/c}]$ and in $p = y^+/h_1/[1 + y^+/h_1]$ (see reference [25]), this means we have $G_* = (Re_\tau/a)^{b/c}/[1 + (Re_\tau/a)^{b/c}]$ and $p_* = Re_\tau/h_1/[1 + Re_\tau/h_1]$. The model that results from the combination of Eqs. (S.1) and (S.3) provides an analytical model for the bulk velocity (PVM-Ub). A corresponding analytical model for the skin-friction coefficient based on the bulk velocity (PVM-Cf) is given by $C_f = 2/U_b^{+2}$, and an analytical model for the Reynolds number based on the bulk velocity (PVM-Re) is given by $Re = 2Re_\tau U_b^+$.

Figure S.1a shows the I_{12} variation according to Eq. (S.3). For $Re_\tau \geq 500$, we see that I_{12} deviates by less than 5% from the asymptotic value one. Asymptotically, we find for channel flow

$$U_{b\infty}^+ = U_\infty^+ - \kappa^{-1}(1 + I_3) = \kappa^{-1}(\ln Re_\tau + C - 1 - I_3) = \kappa^{-1}\ln(3Re_\tau), \quad (\text{S.4})$$

which recovers $U_b^+ = \kappa^{-1}(\ln Re_\tau - 1) + B$. Correspondingly, we find for pipe flow

$$U_{b\infty}^+ = \kappa^{-1}\ln(3.52Re_\tau), \quad (\text{S.5})$$

and for the TBL

$$U_{b\infty}^+ = \kappa^{-1}\ln(5.69Re_\tau). \quad (\text{S.6})$$

For channel flow, we find that the relative error of $U_{b\infty}^+$ compared to U_b^+ is (0.64, 0.41, 0.06, 0.007)% for $Re_\tau = (500, 10^3, 10^4, 10^5)$, respectively, see also Fig. 8 in Sect. 4.2.

Next, let us discuss implications for the skin-friction coefficient and bulk Reynolds number. In the following we will focus on channel flow to restrict the following discussion. The skin-friction coefficient based on the bulk velocity is $C_f = 2/U_b^{+2}$, and $Re = 2Re_\tau U_b^+$ refers to the bulk Reynolds number, which is based on the bulk velocity. Figure S.1b shows C_f versus Re for $Re_\tau \geq 500$ obtained by the PVM-Cf and from experiments [31]. Also shown are the skin friction model $C_f = 0.073/Re^{1/4}$ of Dean [54] and the model $C_f = 0.0743/Re^{1/4}$ of Zanoun et al. [55]. Overall, it may be seen that there is an excellent agreement between the PVM-Cf and the experiments. A discussion of the 95% confidence intervals of measured data can be found elsewhere [31]. It turns out that measured data for relatively small Reynolds numbers are more affected by uncertainty than measured data for relatively high Reynolds numbers. For relatively high Reynolds numbers, the PVM-Cf performs better than the models of Dean [54] and Zanoun et al. [55]. There is only a very minor difference between the latter models.

Figure S.2a addresses the asymptotic variation of the skin-friction coefficient: the curve seen in Fig. S.1b is compared with the curve based on Eq. (S.4), this means

$$C_{f\infty} = \frac{2\kappa^2}{[\ln(3Re_\tau)]^2}. \quad (\text{S.7})$$

There is only a very minor difference between the two curves for relatively low Reynolds numbers: the relative $C_{f\infty}$ error (which is twice the $U_{b\infty}^+$ error) is below 1.3%, which is the maximum error at $Re_\tau = 500$. Hence, the asymptotic C_f variation is governed by Eq. (S.7). The most relevant conclusion of the comparison with the models of Dean [54] and Zanoun et al. [55] is that the asymptotic C_f variation is not well described by a power function: according to Eq. (S.7) it follows an inverse quadratic logarithmic function. An interesting discussion of C_f variations based on different approaches for several flows can be found elsewhere [56]. In contrast to the findings presented here, Pirozzoli's [56] discussion reveals the problem to explain the consistency of assumed

asymptotic and non-asymptotic (Re_τ dependent) C_f variations based on several models and model parameters, i.e. the manifestation of asymptotic C_f profiles.

Figure S.2b addresses the asymptotic $Re - Re_\tau$ relationship. Like in Fig. S.2a, we compare the curve obtained from the PVM-Re with the curve that uses Eq. (S.4), i.e.,

$$Re_\infty = 2\kappa^{-1}Re_\tau \ln(3Re_\tau). \quad (\text{S.8})$$

For the Re_τ range considered there is basically no difference between these functions (the relative Re_∞ error is equal to the $U_{b\infty}^+$ error). Figure S.2b shows that Re_∞ and Re_τ are basically related by a power law. This view can be made more explicit by approximating $\ln(3Re_\tau)$ by the power function aRe_τ^b , where a and b are determined by the condition that the function value and derivative of aRe_τ^b at a certain reference point $Re_{\tau 0}$ are equal to the corresponding $\ln(3Re_\tau)$ values. This results in

$$Re_\infty = 2a\kappa^{-1}Re_\tau^{1+b}, \quad (\text{S.9})$$

where $b = 1/\ln(3Re_{\tau 0})$ and $a = Re_{\tau 0}^{1-b}/b$. For example, for $Re_{\tau 0} = 510$ we obtain $Re_\tau = 0.09Re_\infty^{0.88}$, which is the $Re_\infty - Re_\tau$ relationship quoted by Pope [45]. For a given Re_∞ , Eq. (S.8) can be used to find Re_τ by iteratively solving $Re_\tau = \kappa Re_\infty / [2\ln(3Re_\tau)]$ starting with $Re_\tau = 0.09Re_\infty^{0.88}$ on the right-hand side. A converged solution is obtained in less than four iterations.

S.2. Turbulence Production and Turbulent Viscosity

Let us continue with the discussion of the asymptotic flow structure by considering turbulence characteristics. We consider two relevant combinations of the Reynolds shear stress $\langle u'v' \rangle^+$ and shear rate S^+ : the production $P^+ = -\langle u'v' \rangle^+ S^+$ of turbulent kinetic energy and the turbulent viscosity $\nu_t^+ = -\langle u'v' \rangle^+ / S^+$.

To prepare the discussion of the production $P^+ = -\langle u'v' \rangle^+ S^+$, let us consider some consequences of the analytical production model PVM-P derived here. As it is well known and shown below, relevant variations of P^+ take place very close to the wall. This supports the idea to identify a universal production limit which is only a function of y^+ , i.e., unaffected by Re_τ . For all three flows considered, this universal production limit is given by $P_\infty^+ = -\langle u'v' \rangle^+ S^+ = -(S^+ - M)S^+$, where $M = 1$ (because $M_{CP} = M_{BL} = 1$ close to the wall, see $M_{CP} = 1 - y$, $M_{BL} = e^{-y^6 - 1.57y^2}$) and $S^+ = S_1^+ + S_2^+$ (because wake effects to not affect this flow region). Hence, P_∞^+ is given by

$$P_\infty^+ = S_1^+ + S_2^+ - (S_1^+ + S_2^+)^2 = \frac{1}{4} - \left(\frac{1}{2} - [S_1^+ + S_2^+] \right)^2. \quad (\text{S.10})$$

Hence, the maximum of P_∞^+ is attained at $S_1^+ + S_2^+ = 1/2$, this means exactly at the half of the variation $1 \geq S_1^+ + S_2^+ \geq 0$. This implies

$$(P_\infty^+)_{max} = 1/4. \quad (\text{S.11})$$

The maximum y^+ value y_{max}^+ is obtained by solving $S_1^+ + S_2^+ = 1/2$. It is worth noting that this condition explains the physical relevance of y_{max}^+ as a characteristic shear decay rate. By using $S_1^+ + S_2^+ = 1/2$ in conjunction with the definition of S_1^+ (see reference [25]), y_{max}^+ is found to be given by

$$y_{max}^+ = \frac{a [1/2 + S_2^+(y_{max}^+)]^{1/b}}{\left(1 - [1/2 + S_2^+(y_{max}^+)]^{1/c} \right)^{c/b}}. \quad (\text{S.12})$$

It turns out that the S_2^+ contribution to $S_1^+ + S_2^+ = 1/2$, and, therefore, Eq. (S.12), is very small. This fact allows to solve Eq. (S.12) iteratively starting with $S_2^+ = 0$. The result, which is obtained after only 6 iterations, is $y_{max}^+ = 11.0694$. The latter finding can be also written $y_{max}^+ = 1.0019y_0^+$, where $y_0^+ = 11.0482$ refers to the solution of Eq. (S.12) combined with $S_2^+ = 0$. Hence, there is only a small difference of 0.19% between y_{max}^+ and y_0^+ .

Figures S.3-S.5 show $P^+ = -\langle u'v' \rangle^+ S^+$ as obtained from the PVM-P (this means not P_∞^+) and the production in premultiplied form $\kappa y^+ P^+$ for the three flows considered. The set-up of plots follows Fig. 4 for $\langle u'v' \rangle^+$: DNS data shown at the highest available Re_τ are compared to model predictions at the same Re_τ and $Re_\tau = (10^5, 10^{10})$ to illustrate the Re_τ effect. It may be seen that P^+ is extremely well approximated by P_∞^+ with respect to the three flows considered. Thus, all these P^+ curves are characterized by a maximum production $P^+ = 0.25$ at $y^+ = 11.07$. Hence, P^+ converges asymptotically to P_∞^+ , i.e., P^+ becomes asymptotically independent of the outer scaling variable y . Differences due to the Re_τ considered are seen with respect to the production in premultiplied form $\kappa y^+ P^+$. The consideration of $\kappa y^+ P^+$ is very helpful to reveal contributions to the bulk production: with respect to $\kappa y^+ P^+$, equal areas represent equal contributions to the total production [2,57,58]. The comparison between DNS data and model curves at the corresponding Re_τ shows an excellent agreement with respect to channel flow, and a good agreement for pipe flow and the TBL. This observation simply reflects the accuracy of channel flow versus pipe flow and TBL DNS. Given the excellent reflection of velocities and shear stresses obtained from DNS and the models presented here, it is interesting that there are such differences at all. For the three flows considered, the Re_τ effect shows the expected features: P^+ scales in the log-law region with $1/(\kappa y^+)$, and the extent of the log-law region increases with Re_τ .

In continuation of the production $P^+ = -\langle u'v' \rangle^+ S^+$ discussion, let us consider next the turbulent viscosity $\nu_t^+ = -\langle u'v' \rangle^+ / S^+$, which is equal to the ratio of turbulent to molecular viscosity. To prepare this discussion, let us look at consequences of the analytical turbulent viscosity model PVM-TV. According to the PVM-TV, an exact expression for the turbulent viscosity $\nu_t^+ = -\langle u'v' \rangle^+ / S^+$ is given for channel and pipe flow by

$$\nu_t^+ = \frac{\kappa y^+(1-y)}{\kappa y^+(S_1^+ + S_1^{CP} + S_2^+ + S_2^{CP}) - 1 + G_{CP}(1-y)} - 1. \quad (\text{S.13})$$

For the TBL, the corresponding exact expression $\nu_t^+ = -\langle u'v' \rangle^+ / S^+$ can be written

$$\nu_t^+ = \frac{\kappa y^+ M_{BL}}{\kappa y^+(S_1^+ + S_1^{CP} + S_2^+ + S_2^{CP}) - 1 + G_{BL}} - 1. \quad (\text{S.14})$$

These two expressions for ν_t^+ reveal that ν_t^+ scales with Re_τ for large Reynolds numbers, where the last terms (negative one) in Eqs. (S.13), (S.14) do not contribute. By using the definition $Re_\tau = u_\tau \delta / \nu$, we have $\nu_t^+ / Re_\tau = \nu_t / (\nu Re_\tau) = \nu_t / (u_\tau \delta)$, this means the dimensional turbulent viscosity scales with the outer scales u_τ and δ . This confirms the validity of using u_τ as outer velocity scale, see the discussion by Kim [46].

Let us ask which universal viscosity models for ν_t^+ / Re_τ can be expected. First, we look at the asymptotic features. The way to accomplish this is to consider the asymptotic variations $\kappa y^+ S_1^+ = 0$ and $\kappa y^+ S_2^+ = 1$ in Eqs. (S.13), (S.14), and to neglect correspondingly the last terms (negative one). By using these assumptions we obtain for channel and pipe flow

$$\nu_t^{+as} = \frac{\kappa y^+}{G_{CP}}, \quad (\text{S.15})$$

and for the TBL we obtain

$$\nu_t^{+as} = \kappa y^+ \frac{M_{BL}}{G_{BL}}. \quad (\text{S.16})$$

Here, the superscript *as* refers to the fact that we consider asymptotic profiles. Like G_{CP} and G_{BL} , $M_{BL} = e^{-y^6 - 1.57y^2}$ is only a function of y .

Plots of these viscosity profiles are shown in Fig. S.6. The set-up of plots follows again Fig. 4 for $\langle u'v' \rangle^+$: DNS data shown at the highest available Reynolds number are compared to model predictions at the same Re_τ . Also shown in these plots are the universal asymptotic viscosity limits given by Eqs. (S.15), (S.16), and the curve $Re_\tau^{-1}\nu_t^+ = \kappa y$. It is of interest to see again the influence of inaccuracies on pipe flow and TBL DNS: see the oscillations of $Re_\tau^{-1}\nu_t^+$ for relatively large y values. It may be seen that $Re_\tau^{-1}\nu_t^+ = \kappa y$ appears to be an excellent model except in the wake region. After the $Re_\tau^{-1}\nu_t^+ = \kappa y$ stage, the turbulent viscosities follow their asymptotic profile depending on the flow considered. For the Reynolds numbers considered, it is remarkable that the Reynolds number effect is very small.

In order to see the accuracy of the outer scaling applied to represent the turbulent viscosity in the near-wall region by ν_t^{+as} , let us consider possible deviations from ν_t^{+as} . In order to do so we introduce a parameter C_μ that may account for such deviations,

$$\nu_{t\infty}^+ = C_\mu \nu_t^{+as}. \quad (\text{S.17})$$

Here, $\nu_{t\infty}^+$ refers to the asymptotic limit of ν_t^+ . Plots of C_μ are shown in inner scaling for the three flows considered in Fig. S.6d for $Re_\tau = (500, 10^3, 10^4)$ by calculating $\nu_{t\infty}^+$ in Eq. (S.17) according to Eqs. (S.13), (S.14). For sufficiently large Re_τ , as given for $Re_\tau = 10^4$, C_μ converges to

$$C_\mu^\infty = \frac{1}{\kappa y^+ (S_1^+ + S_2^+)} - \frac{1}{\kappa y^+}, \quad (\text{S.18})$$

which is only a function of y^+ . The latter expression follows from Eqs. (S.13), (S.14) by neglecting outer scaling effects. The limit Eq. (S.18) approaches asymptotically one, as may be seen by using $\kappa y^+ S_1^+ = 0$ and $\kappa y^+ S_2^+ = 1$. For the smaller Re_τ considered, there are very minor deviations of C_μ from C_μ^∞ . Overall, we find that the self-similarity relation $\nu_{t\infty}^+ = C_\mu^\infty \nu_t^{+as}$ represents an excellent approximation for $Re_\tau \geq 500$ as considered.

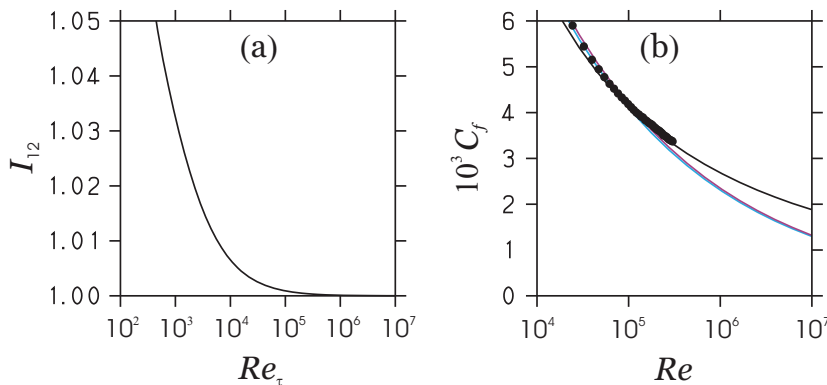


Figure S.1. Bulk flow properties: Figure (a) shows I_{12} obtained from Eq. (S.3). Figure (b) shows C_f according to the PVM-Cf (black line), the model $C_f = 0.073/Re^{1/4}$ of Dean [54] (cyan line) and the model $C_f = 0.0743/Re^{1/4}$ of Zanoun et al. [55] (purple line). The black dots show experimental data [31].

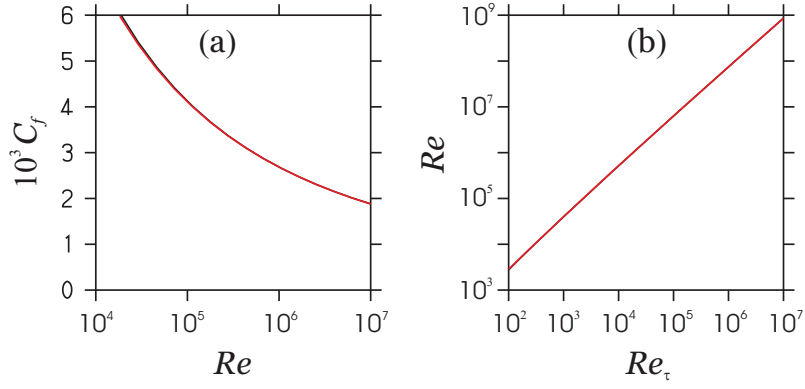


Figure S.2. Bulk flow properties: Figure (a) shows C_f according to the PVM-Cf (black line) compared to $C_{f\infty}$ according to the asymptotic Eq. (S.7) (red line). Figure (b) shows the $Re - Re_\tau$ relationship obtained from the PVM-Re (black line) compared to the asymptotic relationship Eq. (S.8) (red line).

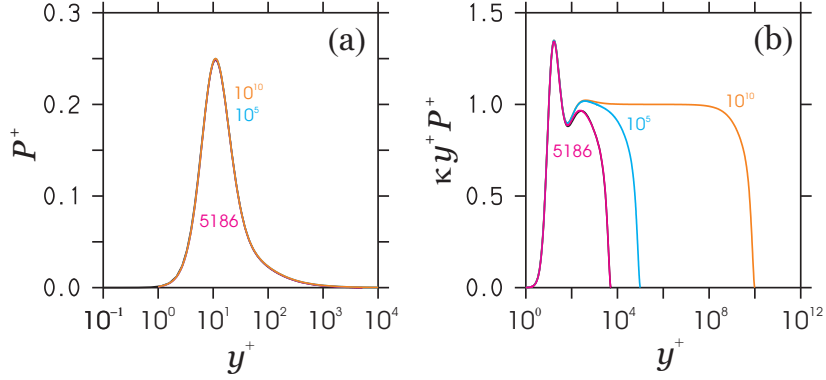


Figure S.3. Channel flow: P^+ and $\kappa y^+ P^+$ are shown in (a) and (b), respectively, according to DNS data of Lee & Moser [26,27] for $Re_\tau = 5186$ (black lines) in comparison to PVM-P predictions for $Re_\tau = (5186, 10^5, 10^{10})$ shown by magenta, cyan, and orange lines, respectively.

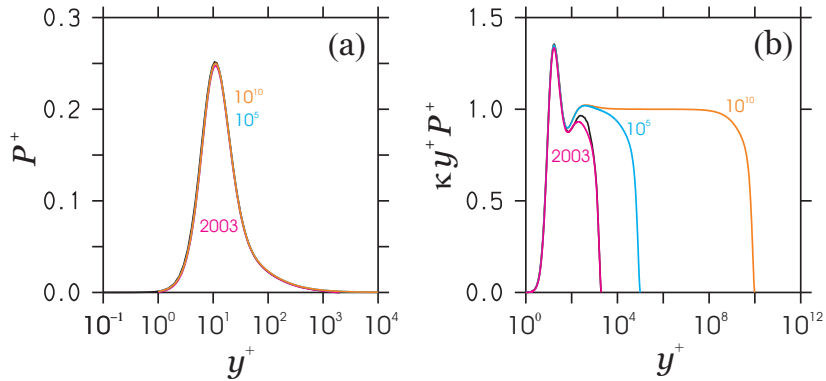


Figure S.4. Pipe flow: P^+ and $\kappa y^+ P^+$ are shown in (a) and (b), respectively, according to DNS data of Chin et al. [28] for $Re_\tau = 2003$ (black lines) in comparison to PVM-P predictions for $Re_\tau = (2003, 10^5, 10^{10})$ shown by magenta, cyan, and orange lines, respectively.

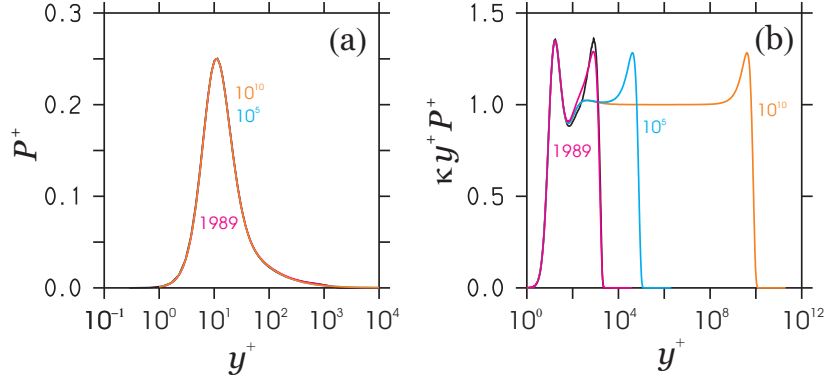


Figure S.5. TBL: P^+ and $\kappa y^+ P^+$ are shown in (a) and (b), respectively, according to DNS data of Sillero et al. [29,30] for $Re_\tau = 1989$ (black lines) in comparison to PVM-P predictions for $Re_\tau = (1989, 10^5, 10^{10})$ shown by magenta, cyan, and orange lines, respectively.

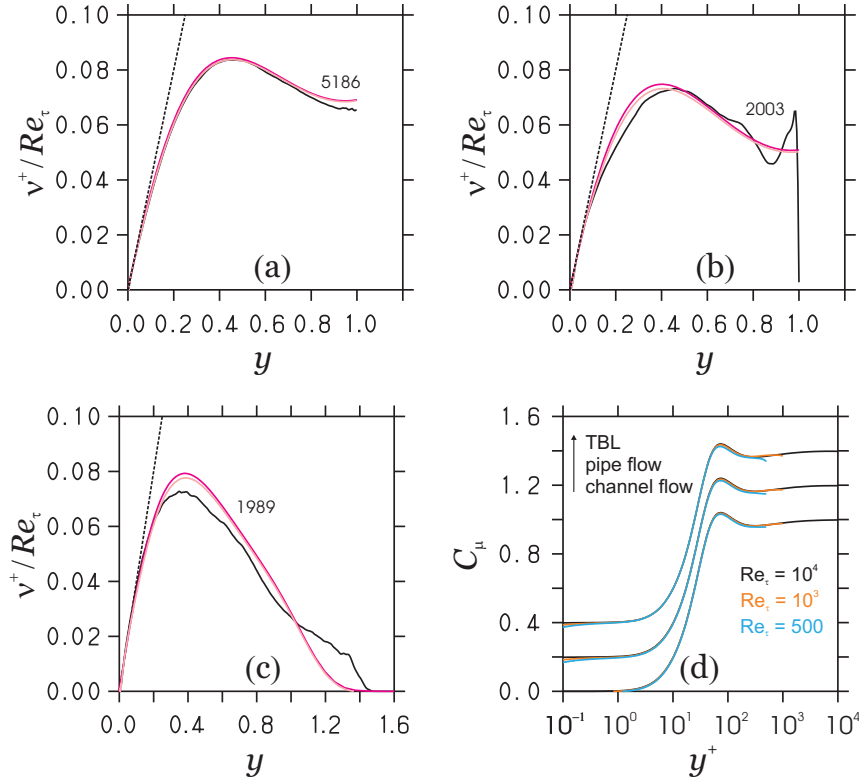


Figure S.6. DNS (black lines) versus model comparisons of ν_t^+ / Re_τ : (a) channel flow DNS data of Lee & Moser [26,27] at $Re_\tau = 5186$; (b) pipe flow DNS data of Chin et al. [28] at $Re_\tau = 2003$; (c) TBL DNS data of Sillero et al. [29,30] at $Re_\tau = 1989$. The model curves (magenta lines) present the asymptotic profiles Eqs. (S.15), (S.16). The pink lines show the corresponding exact PVM-TV profiles, which include Re_τ effects. The black dashed lines show $Re_\tau^{-1} \nu_t^+ = \kappa y$. Figure (d) shows C_μ calculated from Eq. (S.17) for given Re_τ and the three flows considered. The pipe and TBL curves are separated by $\Delta C_\mu = +0.2$, respectively. The $Re_\tau = 10^4$ curves do not show visible differences to the asymptotic limit Eq. (S.18).